PCCP

ARTICLE TYPE

Cite this: DOI: 00.0000/xxxxxxxxxx

A Comprehensive Study of the Molecular Vibrations in Solid-State Benzylic Amide [2]Catenane†

Carlos Romero-Muñiz,*[a] Denís Paredes-Roibás,[b] Antonio Hernanz,[b] and José María Gavira-Vallejo[b]

Received Date
Accepted Date

DOI: 00.0000/xxxxxxxxxx

The interpretation of vibrational spectra is often complex but a detailed knowledge of the normal modes responsible for the experimental bands provides valuable information about the molecular structure of the sample. In this work we record and assign in detail the infrared (IR) spectrum of the benzylic amide [2]catenane, a complex molecular solid displaying crimped mechanical bonds like the links of a chain. In spite of the large size of the unit cell, we calculate all the vibrational modes of the catenane crystal using quantum first-principles calculations. The activity of each mode is also evaluated using the Born effective charges approach and a theoretical spectrum is constructed for comparison purposes. We find a remarkable agreement between the calculations and the experimental results without the need to apply any further empirical correction or fitting to the eigenfrequencies. A detailed description in terms of the usual internal coordinates is provided for over 1000 normal modes. This thorough analysis allows us to perform the complete assignment of the spectrum, revealing the nature of the most active modes responsible for the IR features. Finally, we compare the obtained results with those of Raman spectroscopy, studying the effects of the rule of mutual exclusion in vibrational spectroscopy according to the different levels of molecular symmetry embedded in this mechanically interlocked molecular compound.

1 Introduction

Vibrational spectroscopy is currently an essential tool in chemistry and materials science, widely used to characterize either organic or inorganic materials. Moreover, it is useful to analyze gas phase, liquid, solutions and solid-state samples. Vibrational spectra are very specific to the studied materials and highly sensitive to minor structural changes in the chemical bonding. For this reason, they can provide valuable information at qualitative and quantitative levels. The interpretation of vibrational spectra is generally done by assigning the experimental peaks to the corresponding molecular vibrational modes. Although empirical models and group theory can be used for this purpose, in systems with a high number of normal modes this task becomes rather difficult.

In this work we focus on a challenging molecular solid whose vibrational spectrum is far from being trivial: the benzylic amide [2]catenane. It belongs to the large family of mechanically interlocked molecular architectures,[1,2] and was obtained for the first time in the mid 90's following a template-directed synthesis.[3,4] This compound consists of two identical macrocycles that are mechanically interlocked with a structure resembling a chain. Despite their structural complexity, catenanes and other related compounds have been extensively studied with special emphasis in the internal dynamics of the macrocycles which show a variety of motions.[5–8] These investigations served as a platform for the subsequent development of the molecular machines,[9,10] generating a great scientific and technological interest.

In our previous work,[11] we studied in detail the Raman spectrum of the benzylic amide [2]catenane and now, we turn our attention to the IR spectrum and other relevant structural aspects of this compound. In this regard, this new work completes the total assignment of the vibrational spectrum of the catenane including a comparative study between both spectroscopic techniques. Furthermore, we have analyzed over 1000 vibrational normal modes to draw a comprehensive picture of the vibrational spectra of the catenane that could be useful in future studies devoted to related compounds.

First-principles calculations are especially appropriate to carry out the systematic assignment of vibrational spectra following a normal mode analysis. We use periodic plane-wave density func-

[a] *Departamento de Física Teórica de la Materia Condensada, Universidad Autónoma de Madrid, E-28049 Madrid, Spain*

[b] *Departamento de Ciencias y Técnicas Fisicoquímicas, Facultad de Ciencias, Universidad Nacional de Educación a Distancia (UNED), Paseo de la Senda del Rey 9, E-28040 Madrid, Spain*

* *Electronic address: carlos.romero@uam.es*

† Electronic Supplementary Information (ESI) available: A description of over 1000 normal modes in terms of the usual internal vibrational coordinates in Tables S1 and S2. See DOI: 10.1039/cXCP00000x/

tional calculations to obtain the equilibrium geometry for the solid-state catenane unit cell. Then, we use finite differences to calculate the vibrational normal modes, under the harmonic approximation. And finally, the IR activities of the discrete modes are evaluated through the Born effective charges. This approach was used for the first time to unveil the IR spectrum of fullerene C_{60}.[12] Since then, it has been successfully applied to calculate the IR spectra of a number of substances like carbon nanotubes,[13] oxides,[14] different species adsorbed on surfaces,[15–18] organometallic systems[19,20] or molecular crystals.[21–23] In general terms, this method provides a good accuracy but usually the normal mode analysis is restricted to systems with a relatively small number of atoms, like those mentioned before. Note that the unit cell of this catenane crystal contains 544 atoms. Even so, the accuracy reached in our calculations allows us a direct comparison with experimental data without any empirical correction or fitting to the eigenfrequencies, widely used even in high-quality calculations.[24]

The general structure of this paper is as follows. First we introduce the experimental details of the measurements and the theoretical methodology used to calculate the IR spectrum. After discussing some interesting aspects of the crystal structure and the inter-molecular interactions, we proceed with the assignment of the experimental IR spectrum. Finally, we make a critical comparison between the IR and Raman spectra of the catenane, paying special attention to the rule of mutual exclusion in vibrational spectroscopy, which is partially fulfilled in our case.

2 Experimental and computational methods

2.1 IR spectroscopy

The synthesis of the benzylic amide [2]catenane was made as described in our previous work,[11] following the simple route proposed by Fanti et al.[25] 1.6 mg of the product was powdered, mixed with 301.9 mg of KBr and pressed in a pellet to obtain the infrared spectrum, leading to a weight concentration around 0.53% of the catenane in the pellet.

The equipment used to record the infrared spectrum was a Fourier transform spectrometer Perkin Elmer model Spectrum BX FTIR equipped with a KBr beam splitter with a Michelson interferometer and a DTGS detector. Up to 32 scans were accumulated in order to achieve spectra with an acceptable signal-to-noise ratio with a resolution of 1 cm^{-1} The spectrum was recorded from 450 to 4000 cm^{-1}. Also a blank KBr pellet was used to record the spectral background after 30 minutes of purge with dry N_2 gas circulating in the sample chamber to reduce the CO_2 band around 2340 cm^{-1}. In these conditions an appropriate absorbance value of ~ 0.7 units at the maxima of the bands at 1531 and 1637 cm^{-1} was obtained. Baseline correction using the "End-weighted" algorithm of the OriginPro® 8.0724 software, choosing around 20 points in spectrum was performed. No other numerical treatment or correction (smoothing, shifting, deconvolution, etc.) has been applied to the spectra.

2.2 First-principles calculations

In this work the characterization of the crystal structure of benzylic amide [2]catenane has been carried out by means of Density Functional Theory (DFT) calculations using the VASP (*Vienna Ab Initio Simulation Package*) code[26]. A plane-wave basis sets with a cutoff of 400 eV was used together with PAW pseudopotentials[27,28] for all involved species (C, N, O and H). The PBE (Perdew-Burke-Ernzerhof) exchange and correlation functional[29] was employed aided by the Grimme's D3 semi-empirical correction[30], to include possible dispersion interactions. The equilibrium geometry of the catenane crystal was obtained combining electronic self-consistent loops (cutoff 10^{-6} eV) with a conjugate gradient minimization of the structure, until forces upon atoms were less than 0.005 eV/Å. This demanding criterion in forces was used to ensure the reliability of the subsequent normal mode analysis.

The initial geometry was extracted from X-ray diffraction (XRD) measurements[3,31]. This is an orthorhombic unit cell containing four catenane molecules, leading to $136 \times 4 = 544$ total atoms per unit cell. Periodic boundary conditions are used to properly reproduce the three-dimensional molecular packing of the compound. Further details about the crystal structure of this compound are given in Sec. 3.1. All lattice vectors were kept fixed during the ionic relaxation in order to retain the original symmetry of the crystal structure and very minor differences were found between the final equilibrium configuration and the input geometry. The reciprocal space was sampled with a $2 \times 2 \times 2$ Monkhorst-Pack grid[32], due to the large size of the unit cell.

The normal mode analysis was carried out by direct diagonalization of the Hessian matrix according to the classical analysis[33,34]. Under the harmonic approximation, the vibrational eigenmodes of a system constituted by N atoms are obtained after solving the corresponding eigenvalue problem given by

$$\sum_{j=1}^{3N} (f_{jk} - \lambda_{(n)}\delta_{jk}) A_{j,(n)} = 0, \qquad (1)$$

where f_{jk} is the mass-weighted Hessian matrix, $\lambda_{(n)} = (2\pi\nu_{(n)})^2$ are the eigenvalues, related to the frequencies ν_n of the nth mode, and $A_{j,(n)}$ the elements of the corresponding eigenvectors. Note that the index (n) stands for the number of modes, in total $3N-6$. The Hessian matrix is numerically obtained through finite differences by computing the second derivatives of the energy with respect to the atomic positions. The algorithm considers six different displacements (± 0.02 Å) per atom along the three Cartesian components. Notice that this calculation is restricted to the center of the first Brillouin zone (Γ point) and only the vibrational modes associated with the atoms belonging to the unit cell are considered, giving rise to a total of $544 \times 3 - 6 = 1626$ normal modes.

Alternatively, we can change the notation to use some indexes $\alpha, \beta, \cdots = 1,2,3$ exclusively for the Cartesian coordinates while others $\tau_1, \tau_2, \cdots = 1, \ldots, N$ account for the number of atoms in the

system. Thus, the former Eq. (1) must be rewritten as:

$$\sum_{\alpha=1}^{3}\sum_{\tau_1=1}^{N}(f_{\alpha\beta}^{\tau_1\tau_2}-\lambda_{(n)}\delta_{\alpha\beta}\delta_{\tau_1\tau_2})A_{\alpha,(n)}^{\tau_1}=0. \quad (2)$$

The eigenvectors calculated from this equation depend on the atomic masses and they fulfill the following orthormality condition:

$$\sum_{\alpha=1}^{3}\sum_{\tau=1}^{N}A_{\alpha,(n)}^{\tau}A_{\alpha,(m)}^{\tau}=\delta_{nm}. \quad (3)$$

In addition, an arbitrary displacement $U_{\alpha,(n)}^{\tau}$ in the direction of the nth eigenvector can be written as

$$U_{\alpha,(n)}^{\tau}=\sqrt{m_\tau}Q_{(n)}A_{\alpha,(n)}^{\tau}, \quad (4)$$

where m_τ is the mass of the corresponding atom and $Q_{(n)}$ is referred to as a normal-mode coordinate.

It is well-known that the IR intensity of a normal mode is related to square of the variation of the electric dipole moment μ along the vibration.[33]

$$I_{(n)}^{\mathrm{IR}}=\frac{\rho\pi}{3c}\sum_{\alpha=1}^{3}\left|\frac{d\mu_\alpha}{dQ_{(n)}}\right|^2, \quad (5)$$

where ρ is the molecular volume concentration, c is the speed of light in vacuum and μ_α are the Cartesian components of the electric dipole moment. The derivative along the normal mode can be expressed also with respect to the usual Cartesian atomic coordinates R_α^τ using the eigenvectors.[35]

$$I_{(n)}^{\mathrm{IR}}=\frac{\rho\pi}{3c}\sum_{\alpha=1}^{3}\left|\sum_{\beta=1}^{3}\sum_{\tau=1}^{N}\frac{\partial\mu_\alpha}{\partial R_\beta^\tau}A_{\beta,(n)}^{\tau}\right|^2. \quad (6)$$

From a practical point of view the IR intensity of the modes can be expressed in terms of the Born effective charges, a second rank tensor, defined as the linear change in the polarization vector component P_α per unit cell when the atom τ is displaced along the β axis.[36,37] That is:

$$Z_{\alpha\beta,\tau}^{*}=\frac{\Omega}{e}\frac{\partial P_\alpha}{\partial R_\beta^\tau}, \quad (7)$$

where Ω is the volume of the unit cell and e the electron charge.

Notice that the Born effective charges, together with other relevant electronic properties, can be calculated within DFT methods in the frame of the linear response theory using Density Functional Perturbation Theory (DFPT).[37,38] Using the definition of the Born effective charges, and the direct relation between the electric dipole moment and the polarization vector, the IR intensity per mode can be calculated as

$$I_{(n)}^{\mathrm{IR}}\propto\sum_{\alpha=1}^{3}\left|\sum_{\beta=1}^{3}\sum_{\tau=1}^{N}Z_{\alpha\beta,\tau}^{*}A_{\beta,(n)}^{\tau}\right|^2. \quad (8)$$

Finally, once the intensity of all modes has been calculated, a discrete collection of intensities associated with each normal mode is obtained and the complete spectrum can be constructed as a sum of continuous Lorentzian functions centered in each eigenfrequency. A smearing of $\gamma=3$ cm^{-1} is enough to achieve a good resolution and proceed with the assignment but a high value ($\gamma=50$ cm^{-1}) was used in some parts of the spectrum to reproduce the experimental conditions.

We would like to remark that this approach to calculate the IR spectrum neglects the anharmonicity since we are exclusively dealing with the vibrational ground state under the harmonic approximation. Thus, typical anharmonic effects such as overtones and combination bands fall beyond our analysis although the use of the D3 semi-empirical correction could minimize the expected underestimation of harmonic wavenumbers. Furthermore, the influence of anharmonicity is sometimes noticeable in small organic molecules, but it is usually rather weak in large-size molecular systems.[39] Of course, there are methods available to take into account properly the anharmonicity.[40–42] However, the large size of our system together with the expected little influence of its effects prevent us to perform a fully anharmonic calculation, whose computational cost would be unaffordable at present.

3 Results and discussion

3.1 Structure and energetic considerations

The crystal structure of the benzylic amide [2]catenane was experimentally disclosed in 1995 by Johnston et al.[3]. This compound crystallizes with orthorhombic symmetry (space group *Pbcn*), and its unit cell ($a=17.4382$ Å, $b=12.4628$ Å, $c=23.6926$ Å) contains four catenane molecules. This crystal lattice, shown in Fig. 1, can be visualized as a layered structure along the z direction linked via hydrogen bonds and other dispersion forces. This peculiar arrangement has the ability of maximizing both inter- and intra-molecular π-stacking interactions.

The isolated gas-phase catenane molecule consists of two identical 68-atom macrocycles mechanically interlocked. Each of them, in turn, is constituted by four bound aromatic subunits (–C_6H_4–CO–NH–CH_2–) or (–C_6H_4–CH_2–NH–CO–), linked in *meta* or *para* positions. Notice that the stability of the isolated macrocycles is certainly low due to the lack of a noticeable planar rigidity in its molecular structure, unlike other fully aromatic macrocycles, such as phthalocyanines or porphyrins. Thus, the stabilization of the catenane molecule comes from the formation of six hydrogen bonds per catenane unit, as a consequence of the mechanical bond. Although there is a considerable variability depending on the involved species, the energy of a single NH$\cdots$O=C hydrogen bond in secondary amides (for example in N-methylacetamide) is about 0.22 eV.[43–45] Our calculations point out an energy gain of 1.28 eV per macrocycle in the catenane molecule with respect to the isolated macrocycles. This result is fully consistent with the creation of six hydrogen bonds.

In the solid state, all macrocycle units of the catenane are structurally and conformationally identical, as demonstrated by XRD experiments.[3] Hence, our analysis is restricted to one of these equivalent units. In Table 1 we have collected some relevant structural parameters of the catenane crystal structure and compared to their XRD experimental counterparts. The agreement between the equilibrium geometry obtained through DFT calculations and the experimental values is remarkable. For instance,

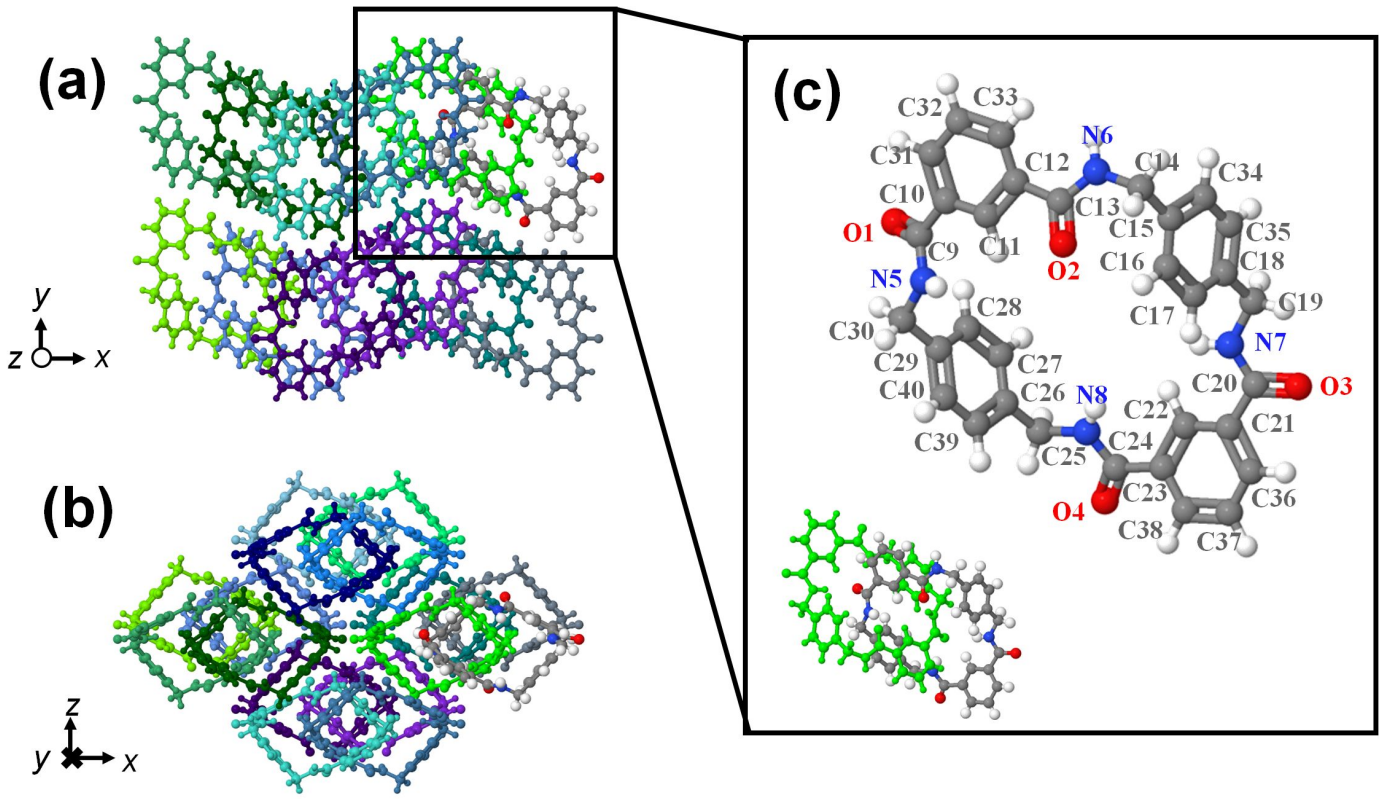

Fig. 1 Crystal structure of the benzylic amide [2]catenane: Ball-and-stick model of the solid-state structure of the catenane showing a top view (a) and a side view (b) of the crystal packing of the molecules. Notice that each macrocycle is drawn in a different color to facilitate the visualization. One of them is depicted with the usual CPK color code, which is magnified in (c) with the atoms labeled as in ref. 3 to compare some relevant structural parameters collected in Table 1.

the variations of bond lengths involving N and O atoms remain smaller than 0.03 Å, leading to relative errors below 2.5% in the worse cases. The same general trend is observed for the bond angles in which the maximum deviations are as large as 2.5%, being in most of the cases less than 1%. Lastly, even for dihedral angles the concordance is very high, taking into account that this crystallographic parameter is very sensitive to minor changes in the structure. In all cases the deviations are smaller than 5%. The comparison summarized in Table 1 is a proof of the high accuracy achieved in the structure optimization.

The driving force that governs the assembly of the catenane crystal lattice is mainly intermolecular hydrogen bonding between adjacent units but $\pi-\pi$ interactions between aromatic rings have also an important role in the three-dimensional packing. Every aromatic ring belonging to the catenane units adopts a close to parallel configuration with respect to another neighboring ring along the x-axis, as depicted in Fig. 1a. In this way, the favorable electrostatic interactions arising from the $\pi-\pi$ stacking are maximized, leading to a noticeable stability of the whole structure. In addition, the catenane layers hold together along the z axis by two intermolecular hydrogen bonds and other dispersion interactions, as depicted in Fig. 2. These interlayer hydrogen bonds are formed between the amide groups pointing outwards of the macrocycles and the corresponding carbonyl groups of some nearest neighbor cycle of the following layer, as shown in Fig. 2. Notice that both macrocycles of each catenane unit are involved in this complex hydrogen bonding architecture. For instance, in the catenane highlighted in Fig. 1c the hydrogen bonds corresponding to that macrocycle would be located at N6-H and O4 atoms.

The energy variation of the solid-state structure with respect to the isolated macrocycles is as large as 3.55 eV per macrocycle. In this energetic balance we have to take into account the hydrogen bonding and the $\pi-\pi$ interactions, whose interaction energy is ~ 0.1 eV in a benzene dimer.[46,47] However, this value can be significantly enhanced, even twice, in benzene derivatives,[48,49] which is precisely the case of the aromatic rings of the catenane molecules. Then, 1.55 eV of the energy gained in the crystal structure can be attributed to the formation of seven hydrogen bonds per cycle (considering also the extra inter-catenane hydrogen bond) while up to ~ 1 eV arise from the $\pi-\pi$ interactions (four interacting rings per cycle). The remaining ~ 1 eV is a consequence of other dispersion interactions which are significantly relevant in this case because of the larger size of the system.

Unfortunately, the insensitivity of X-ray scattering to H atoms prevents us to make a comparative study of the structural parameters of H-bonds but our calculations suggest that inter-catenane H-bonds are slightly stronger than the intra-catenane ones. This is because the bond lengths are slightly shorter: 1.85 Å compared to $2.0-2.2$ Å for intra-catenane bonds.

Table 1 Selected bond lengths, bond angles and dihedral angles of the bencylic amide [2]catenane crystal. All parameters are refered to the same macrocycle of the solid-state structure, as shown in Fig. 1 and compared with X-ray diffraction measurements carried out by Johnston et al.[3]

Bond length (Å)	Exp. (ref. 3)	This work	Error (%)
O1-C9	1.261	1.259	0.16
O2-C13	1.226	1.256	-2.45
O3-C20	1.241	1.249	-0.64
O4-C24	1.224	1.254	-2.45
N5-C9	1.321	1.348	-2.04
N5-C30	1.466	1.455	0.75
N6-C13	1.353	1.350	0.22
N6-C14	1.472	1.465	0.48
N7-C19	1.453	1.454	-0.07
N7-C20	1.336	1.358	-1.65
N8-C24	1.339	1.352	-0.97
N8-C25	1.449	1.466	-1.17
Bond angle (°)	Exp. (ref. 3)	This work	Error (%)
O1-C9-C10	119.22	121.1	-1.58
O1-C9-N5	122.15	123.3	-0.94
O2-C13-C12	119.35	120.0	-0.55
O2-C13-N6	122.68	121.9	0.63
O3-C20-C21	119.92	120.4	-0.40
O3-C20-N7	120.22	122.4	-1.82
O4-C24-C23	121.67	120.6	0.88
O4-C24-N8	121.19	121.8	-0.50
N5-C9-C10	118.63	115.6	2.55
N5-C30-C29	115.29	113.1	1.90
N6-C13-C12	117.57	118.0	-0.37
N6-C14-C15	113.27	114.5	-1.09
N7-C20-C21	119.86	117.1	2.30
N7-C19-C18	113.92	113.8	0.10
N8-C24-C23	117.09	117.6	-0.43
N8-C25-C26	113.82	112.7	0.98
Dihedral angle (°)	Exp. (ref. 3)	This work	Error (%)
C11-C10-C9-N5	-27.08	-27.8	-2.65
C11-C10-C9-O5	152.34	150.5	1.21
C10-C9-N5-C30	173.75	175.0	-0.72
C9-N5-C30-C29	109.88	108.0	1.71
N5-C30-C29-C28	63.12	59.6	5.58
C11-C12-C13-N6	-150.14	-154.8	-3.10
C11-C12-C13-O2	22.75	23.9	-5.05
C12-C13-N6-C14	179.82	178.0	1.01
C13-N6-C14-C15	-77.41	-74.6	3.63
N6-C14-C15-C34	-85.92	-86.9	-1.14
C22-C21-C20-N7	-18.62	-19.5	-4.73
C22-C21-C20-O3	160.18	162.0	-1.14
C21-C20-N7-C19	178.02	178.5	-0.27
C20-N7-C19-C18	139.51	138.0	1.08
N7-C19-C18-C17	-30.02	-30.3	-0.93
C22-C23-C24-N8	25.69	26.8	-4.31
C22-C23-C24-O4	-151.93	-155.0	-2.02
C23-C24-N8-C25	178.33	177.1	0.69
C24-N8-C25-C26	-152.77	-153.0	-0.15
N8-C25-C26-C39	91.12	92.6	-1.62

These bond lengths are similar to the ones found in related compounds.[43,44] On the other hand, the bond angles are also consistent with the formation of H-bonds, revealing a marked directionality, with bond angles NH···O between 160° and 175°. In this regard, the inclusion of a dispersion correction is essential for a proper description of the intermolecular interactions of the mechanical bond in this compound.

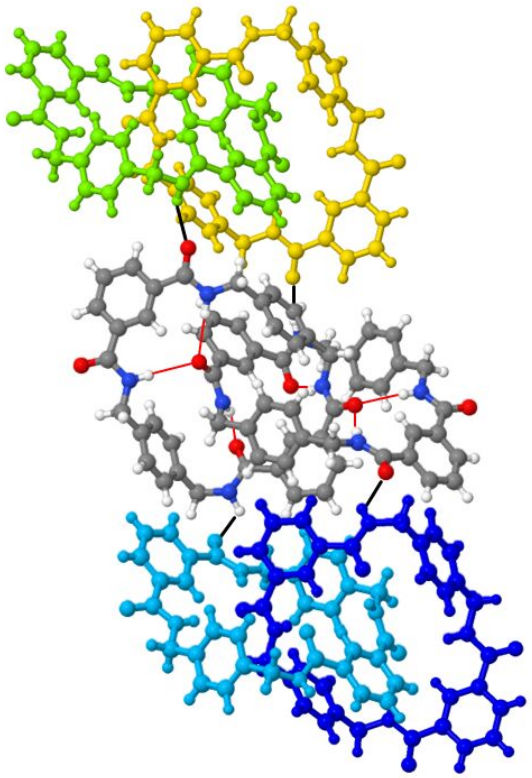

Fig. 2 Perspective view of the stacking structure of the catenane crystal showing the formation of the hydrogen bonds. The intra-catenane hydrogen bonds are represented with red lines while inter-catenane hydrogen bonds are depicted in black.

3.2 Band assignment and description of the modes

Following the procedure detailed in Sec. 2.2, we have evaluated the IR activity of each normal mode of the unit cell of the catenane crystal. To proceed with the systematic assignment of the spectrum we have described more than 1000 normal modes, which are collected in Table S2 of ESI †. We associate each peak of the experimental spectrum with its corresponding peak in the calculated spectrum and the most active discrete modes, which are described in terms of the usual internal coordinates. For practical purposes we have summarized the whole analysis in Table S1 of ESI †by selecting only those modes whose IR activity is larger than 1% with respect to the most active mode. Due to the complex molecular structure of the catenane, each normal mode might not be strictly localized, but it can be qualitatively described as a linear combination of typical simple modes (i.e. stretching, bending, wagging, rocking, etc.) Thus, Tables S1 and S2 collect only a brief description of those internal coordinates that contribute most to the potential energy. Of course there are other minor contributions (vibrations with much smaller amplitudes) that have been omitted for simplicity.

Fig. 1a shows the complete IR spectrum of the bencylic amide [2]catenane experimentally obtained (blue curve) and the corresponding calculation (orange curve). As usual, the experimental spectrum was recorded from ~ 400 cm^{-1}. The calculation is obviously performed in the whole wavenumber range (not shown in Fig. 1). The overall agreement between the calculated and ex-

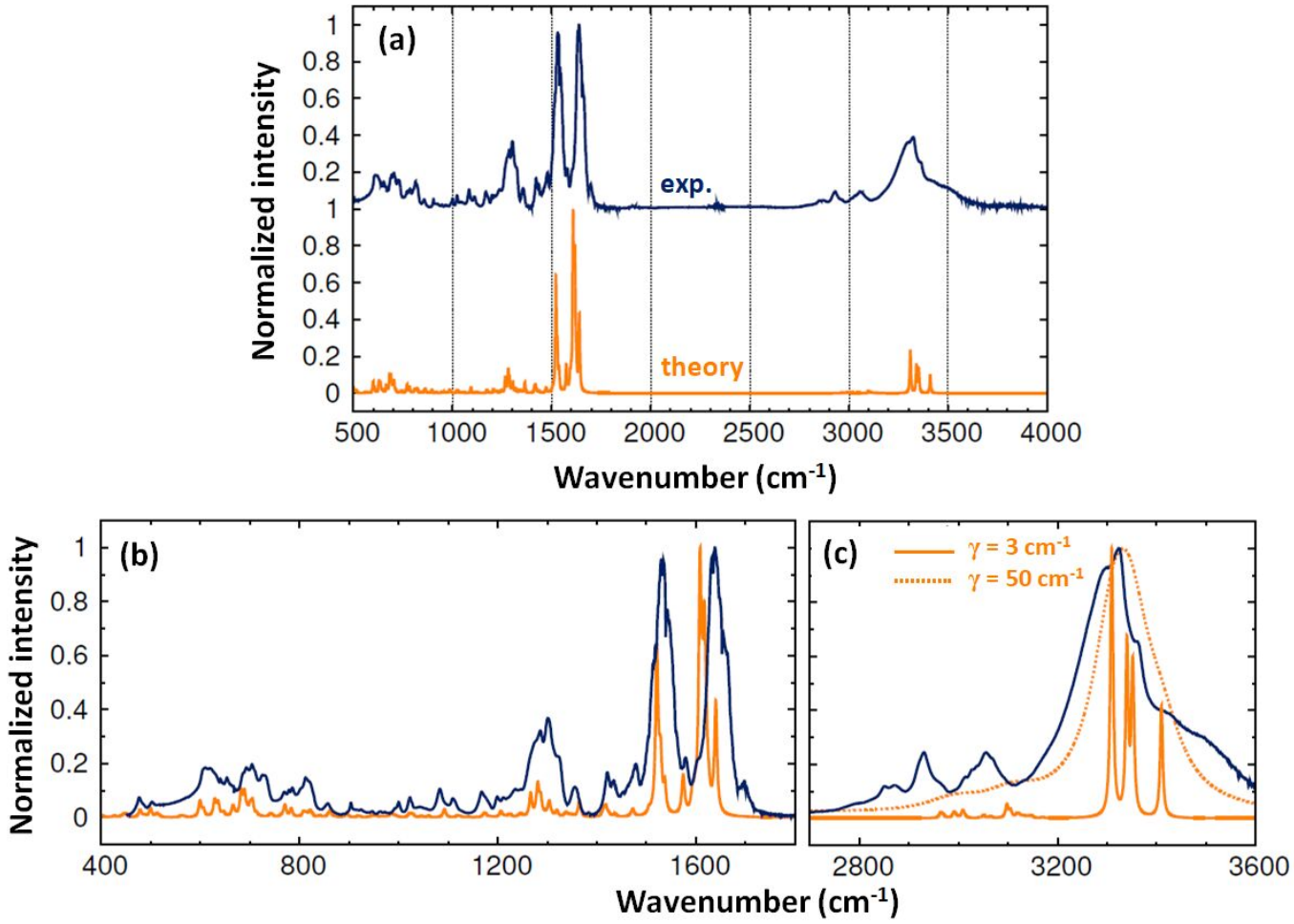

Fig. 3 Experimental and calculated IR whole spectra (a). Superimposed comparison of the experimental and calculated spectra in the low wavenumber region (b) and high wavenumber region (c). Notice that we have used two different smearing values in the high wavenumber region to account for the effect of the hydrogen bonds found in the experiments.

perimental spectra is clear, especially, if we look at the superimposed representations of Figs. 3b and 3c. According to Fig. 3, the interesting IR fingerprints of the catenane are confined in three regions of the spectrum (namely $[600-800]$ cm^{-1}, $[1000-1600]$ cm^{-1} and $[2800-3400]$ cm^{-1}) that we will analyze in detail. Conversely, the very low energy region contains limited and less accessible information about the molecular structure of the sample. Most of the low energy vibrational modes involve crystal phonon modes or complex collective excitations difficult to rationalize with simple geometrical descriptions. However, we would like to remark the presence of a single mode with a high IR activity at 113 cm^{-1} that could be detected using far-IR spectroscopy. This mode is characterized by the out-of-plane bending of the aliphatic chains (πCCCN). Additionally, the wavenumber region between 1700 and 2800 cm^{-1} is fully absent of any relevant IR signal, a common feature in most of organic compounds without unusual atoms.

The low wavenumber region of the spectrum ($600-800$ cm^{-1}) is characterized mainly by the aromatic ring distortions of different nature (i.e. symmetric and antisymmetric modes involving in-plane and out-of plane vibrations). Additional modes present in this region include some in-plane (δCCN or δCNC) and out-of-plane (πCCNH) bending vibrations together with some low-energy stretching on the aromatic rings. Notice that there are no relevant discrete modes in terms of activity in this region but a considerable amount of them displaying a moderate activity. Consequently, a series of weak and broad peaks appear in this region of the spectrum as shown in Fig. 3b.

If we go further in wavenumber ($1000-1600$ cm^{-1}) we can still find benzene ring distortions and bending modes with remarkable activity, giving rise to noticeable peaks at 1083, 1127 and 1182 cm^{-1} (ring distortions) or at ~ 1300 cm^{-1} (δCCN). Other vibrational modes, typical of this wavenumber range, are present but with a low impact in the spectrum. This includes CH_2 torsion, wagging and scissoring modes located at ~ 1220 cm^{-1}, ~ 1350 cm^{-1} and ~ 1420 cm^{-1} respectively. However, in this region of the spectrum the most significant contributions arise from the stretching vibrations of the aliphatic chains, more specifically: νCO, νCN and νCC. The most active peak of the catenane spectrum is located at 1602 cm^{-1} due to the stretch of C=O, with another intense peak at 1630 cm^{-1}. This is a general trend of amides, which possess strong IR bands near 1670 cm^{-1}. In the case of our cate-

nane they appear at lower wavenumbers due to the presence of hydrogen bonds, that are responsible for this shift. Besides, the non-cyclic secondary amide group (O=C−NH−C) not only has a C=O stretch at 1670 cm^{-1}, but another strong band around 1550 cm^{-1} involving bending and stretching modes (δCNH and νCN). This peak is also present in the catenane spectrum at 1530 cm^{-1}, which is, in fact, the second strongest peak in the spectrum (see details in Fig. 3b).

The high energy region of the spectrum ($2800-3400$ cm^{-1}), shown in Fig. 3c, is essentially governed by the stretching vibrations, with a predominant contribution of NH with secondary contributions from CH_2, and CH of the rings. There are also lower contributions of in-plane bending of the aliphatic linkers (δCCN) and stretching (νCN). In particular, two small peaks near 2900 cm^{-1} come from the stretching of CH_2 in combination with in-plane bending of CCN. A similar peak is found at 3050 cm^{-1} as a consequence of ring CH stretching and a very broad band centered at 3350 cm^{-1} due to NH stretching, again accompanied by in-plane bending of CCN and involving also the direct stretching of the NH$\cdots$O hydrogen bonds. It should be pointed out that the CN stretching and CNC bending observed at high frequencies have very low amplitudes and that, rather than genuine vibrational modes, they could be considered movements associated with the elongation/shortening of the NH bonds, whose amplitude is much larger.

The NH stretch band of the spectrum is clearly influenced by the hydrogen bonds and displays features also observed in smaller size compounds containing a set of double NH$\cdots$O hydrogen bonds such as isocyanuric acid, ammeline, uracil, 2-imidazolidone, etc.[39,50] On the one hand, the presence of hydrogen bonds shifts the stretching frequencies of NH (also in the case of OH) to lower values. For this reason, it appears at 3350 cm^{-1} while "free" NH stretching is usually found well above 3400 cm^{-1}. On the other hand, the large broadening of the band is also a well-known consequence of the hydrogen bonds. In fact, if we use a larger smearing to construct the theoretical spectrum the shape of the high wavenumber region becomes very similar to the one found in the experiments, see the dashed line in Fig. 3c. Notice that previous studies[51,52] have already pointed out the importance of hydrogen bonds in this compound and particularly the NH stretch band of the IR spectrum, which is highly sensitive to its chemical environment.[52] This is a spectroscopic fingerprint of the mechanical bond, absent in the isolated macrocycles.

3.3 Further remarks about the whole vibrational spectrum

The rule of mutual exclusion[50] in molecular spectroscopy states that no normal mode can be simultaneously active in IR and Raman spectroscopy if the system is centrosymmetric. This principle does not imply that a Raman inactive vibrational mode must be IR active and vice versa. In fact, there might be modes which are neither Raman nor IR active (silent modes). This rule of thumb summarizes the complementary character of these techniques. However, in the absence of a center of symmetry, this comparative analysis becomes more difficult because the mutual exclusion is not valid anymore and normal modes might be IR and Raman active at the same time. This is the case of many complex-structure compounds like the catenane crystal considered in this work. Fig. 4 compares the IR of the catenane with the Raman spectrum obtained in our previous work.[11] The most relevant peaks are indicated on each spectrum. Although the Raman and IR spectra have been recorded in different experimental conditions, the normal mode analysis is the same and therefore our calculations allow us to make a fair comparison. As it is deduced from Fig. 4, there are a number of peaks that coincide in both techniques while others are only present in one of them. To facilitate the subsequent analysis we have summarized in Table 2 the peaks found in the spectra of Fig. 4 together with a brief geometrical description of the main vibrational modes responsible for each peak.

A good understanding of the whole vibrational spectrum can be achieved only in terms of the crystalline and molecular levels of symmetry displayed by the catenane structure. At solid-state level, the crystallographic unit cell belongs to the space group *Pbcn*, which has a center of symmetry. Although minimum structural variations with respect to the ideal geometry result from the optimization process, they are small enough to consider the optimized unit cell centrosymmetric as well. On the other hand, the molecular structure of the catenane in the unit cell is clearly not centrosymmetric. Nevertheless, a center of symmetry could be considered for each macrocycle embedded in the crystal structure with minimal deviations from the centrosymmetry. In summary, we have a centrosymmetric crystal structure with a non-centrosymmetric molecular motif but constituted, in turn, by nearly centrosymmetric subunits. These levels of molecular symmetry have a direct reflection in the vibrational spectra of the catenane.

The very low wavenumber region of the spectrum is governed by the phonons and lattice vibrational modes as a consequence of the long-range symmetry of the catenane crystal. Since the unit cell has a center of symmetry these low-energy vibrational modes of the catenane crystal should be affected by the rule of mutual exclusion. Unfortunately, most of these modes belong to the sub-400 cm^{-1} region, not analyzed in the IR experiments and strongly affected by the Rayleigh scattering in Raman spectroscopy. Thus, no further information can be extracted in this respect. In any case the calculated IR and Raman activities in this region of the spectra are almost negligible.

For higher wavenumber, the purely molecular modes prevail and we must distinguish between two types of vibrations leading to distinctive behaviors in the vibrational spectra. On the one hand, we can find vibrational modes which do not affect the intermolecular interactions, like the benzene rings distortions. Since aromatic rings do not participate in the intermolecular bonding the signals coming from this kind of modes must fulfill the mutual exclusion rule due to the centrosymmetric nature of the macrocycles. The most representative example can be found at ~ 1000 cm^{-1}, where the strongest band of the Raman spectrum is localized. This strong signal arises from slight planar and non-planar ring deformations, including the typical benzene breathing modes. Conversely, no signal is observed in the equivalent region of the IR spectrum. According to Table 2 other similar ex-

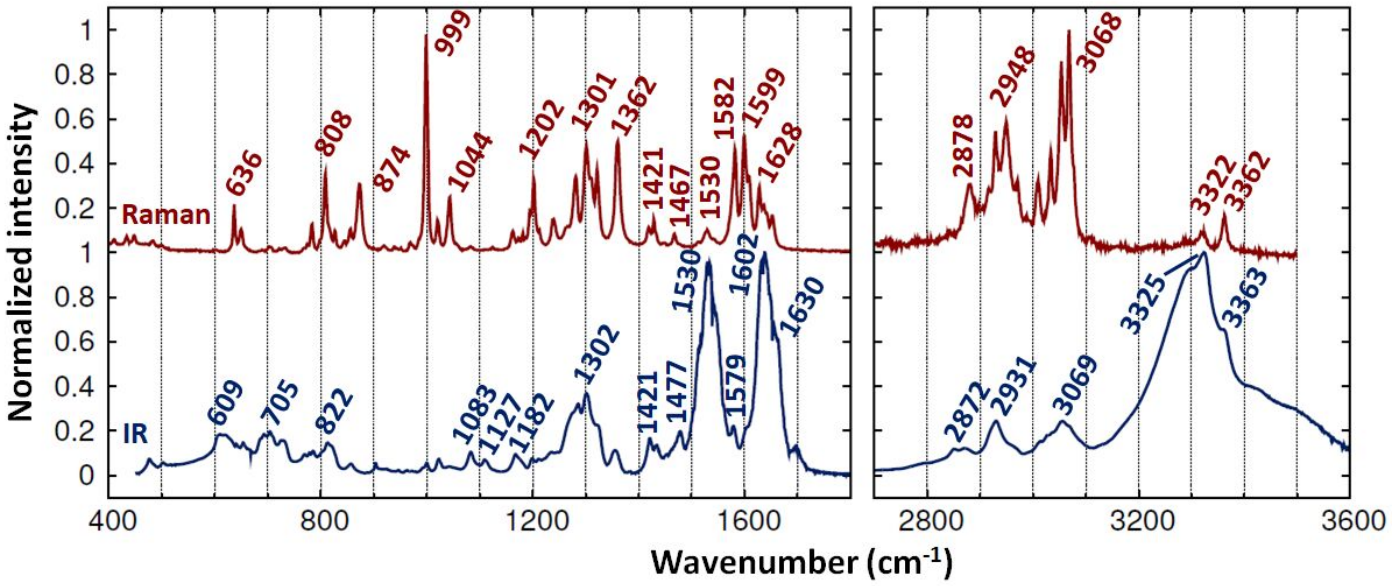

Fig. 4 Detailed comparison of the Raman and IR spectra of the catenane crystal. The wavenumber of the most relevant peaks in cm^{-1} are indicated in each case.

Table 2 Comparison between the main peaks of the experimental IR and Raman spectra. A brief description of the main contributions of each peak is given in terms of the usual internal vibrational coordinates. Internal coordinates: ν, stretching; δ, in-plane bending; π, out-of-plane bending; τ, torsion and ω wagging. Additional labels: a, antisymmetric; r, benzene ring; rd, benzene ring deformation; s, symmetric.

Raman (cm^{-1})	Main modes	IR (cm^{-1})	Main modes
-		609	s-out-of-plane-rd
636	rd	-	
-		705	rd
808	s-in-plane-rd	-	
-		822	s-out-of-plane-rd
874	s-in-plane-rd	-	
999	s-in-plane-rd + s-r-νCH	-	
1044	δCNC + νCN	-	
-		1083	a-in-plane-rd + δCCC
-		1127	s-in-plane-rd
-		1182	s-in-plane-rd
1202	s-in-plane-rd	-	
-		-	
1282	δCCN + a-in-plane-rd	1284	δCCN + νCC + a-in-plane-rd
1301	δCCN + a-in-plane-rd	1302	δCCN + νCC + a-in-plane-rd
1322	νCC + τCH_2	-	
-		1355	a-in-plane-rd
1362	ωCH_2	-	
1421/1429	sci-CH_2 + δCCN + a-in-plane-rd	1421/1439	sci-CH_2 + δCCN + a-in-plane-rd
1467	sci-CH_2 + δCCN + a-in-plane-rd	-	
-		1477	a-in-plane-rd + νCC
1530	νCN	1530	νCN + νCC + δCNH
1582	νCC + δCCN + νCO	1579	νCC + δCCN + νCO
1599	νCO + νCN	1602	νCO + νCC + δCCN + a-in-plane-rd
1628	νCO + νCN	1630	νCO + νCC + νCN
2878	s-νCH_2 + δCCN	2872	s-νCH_2 + δCCN + νCC + νCN
2948	νCH_2 + δCCN + νCN	2931	νCH_2 + δCCN + νCN
3054	r-νCH	3057	r-νCH + in-plane-rd
3068	r-νCH	3069	r-νCH + in-plane-rd
3322	νNH + νCN	3325	νNH + δCNC
3362	νNH + νCN	3363	νNH + δCNC

amples can be found within the 600-1200 cm^{-1} range, where the indicated mutual exclusion is strictly fulfilled.

On the other hand, there are vibrations affecting the groups connecting macrocycles via hydrogen bonds. These modes basically include those localized in the aliphatic chains, namely bending including the N atoms (δCCN) and stretching involving N or O atoms (νCN, νCO and νNH). These vibrations are characteristic of the complete non-centrosymmetric structure of the catenane, and consequently they do not follow the mutual exclusion rule, in contrast with the vibrations of the aromatic rings. Most of the vibrations affecting intermolecular interactions are localized above 1500 cm^{-1} and including also the high wavenumber region > 2900 cm^{-1}. According to Table 2 these modes display a remarkable activity in both spectra. For instance, the amide carbonyl stretch band at ~ 1600 cm^{-1} is the most intense peak of the IR spectrum but at the same time it is clearly visible in the Raman spectrum with a weaker intensity. Similar examples of simultaneous activity are found at ~ 1300 and ~ 1420 cm^{-1} as a consequence of δCCN and at ~ 1530 cm^{-1} from νCN. Finally, in the high wavenumber region the r-νCH and νNH vibrations appear in the IR and Raman spectra located at ~ 3050 and ~ 1600 cm^{-1} respectively. Surprisingly, r-νCH modes are included in the vibrations with twofold activity despite being localized on the aromatic rings. This is because some CH atoms of the ring are rather close to the amide groups and these high energy stretching modes interfere with the NH$\cdots$O hydrogen bonds. We refer for instance to C11H, C28H, C17H or C22H in Fig. 1c, which are involved in these vibrations.

4 Conclusions

In this work, we have carried out a systematic assignment of the whole vibrational spectrum of the solid-state benzylic amide [2]catenane. We have experimentally recorded the IR spectrum of this compound and performed a normal mode analysis by means of quantum first-principles calculations. First, we have discussed at quantitative level the crystal structure of this molecular solid and the energetics of its intermolecular interactions. Then we have analyzed more than 1000 vibrational normal modes in terms of the usual internal coordinates, leading to the full characterization of the experimental IR spectrum. The agreement between the theoretical calculations and the experimental results is very good for wavenumber less than 1650 cm^{-1} while some minor discrepancies appear above 2900 cm^{-1}, likely due to the anharmonicity. As a result, we have unraveled the IR fingerprint of this complex compound, paying special attention to the intermolecular features that can be noticed in the IR spectrum. Finally, we have made a careful comparison between the IR and Raman spectra, concluding that those normal modes affecting the hydrogen bonding of the crystal packing do not fulfill the rule of mutual exclusion in vibrational spectroscopy, while lattice vibrations and the modes entirely enclosed in the macrocyclic subunits do fulfill the mentioned rule. This is a consequence of the different levels of molecular symmetry contained in the complex structure of the catenane crystal. In conclusion, the results presented in this work set a robust and fundamental basis for further studies involving other mechanically interlocked compounds, especially if vibrational spectroscopy techniques are used.

Conflict of Interest

The authors declare no competing financial interest.

Acknowledgements

We gratefully acknowledge Dr. Óscar Gálvez for his technical support and Prof. Rafael Escribano for the critical reading of the manuscript.

Notes and references

1 D. B. Amabilino and J. F. Stoddart, *Chem. Rev.*, 1995, **95**, 2725–2828.
2 F. M. Raymo and J. F. Stoddart, *Chem. Rev.*, 1999, **99**, 1643–1664.
3 A. G. Johnston, D. A. Leigh, R. J. Pritchard and M. D. Deegan, *Angew. Chem. Int. Ed.*, 1995, **34**, 1209.
4 A. G. Johnston, D. A. Leigh, L. Nezhat, J. P. Smart and M. D. Deegan, *Angew. Chem. Int. Ed.*, 1995, **34**, 1212.
5 D. A. Leigh, A. Murphy, J. P. Smart, M. S. Deleuze and F. Zerbetto, *J. Am. Chem. Soc.*, 1998, **120**, 6458.
6 A. M. Brouwer, C. Frochot, F. G. Gatti, D. A. Leigh, L. Mottier, F. Paolucci, S. Roffia and G. W. H. Wurpel, *Science*, 2001, **291**, 2124–2128.
7 F. G. Gatti, S. León, J. K. Y. Wong, G. Bottari, A. Altieri, M. A. Farrán-Morales, S. J. Teat, C. Frochot, D. A. Leigh, A. M. Brouwer and F. Zerbetto, *Proc. Natl. Acad. Sci. USA*, 2003, **100**, 10–14.
8 D. A. Leigh, J. K. Y. Wong, F. Dehez and F. Zerbetto, *Nature*, 2003, **424**, 174.
9 E. R. Kay, D. A. Leigh and F. Zerbetto, *Angew. Chem. Int. Ed.*, 2007, **46**, 72–191.
10 S. Erbas-Cakmak, D. A. Leigh, C. T. McTernan and A. L. Nussbaumer, *Chem. Rev.*, 2015, **115**, 10081–10206.
11 C. Romero-Muñiz, D. Paredes-Roibás, C. Lopez, A. Hernanz and J. M. Gavira-Vallejo, *J. Phys. Chem. C*, 2018, **122**, 18102–18109.
12 P. Giannozzi and S. Baroni, *J. Chem. Phys.*, 1994, **100**, 8537–8539.
13 J. Zhou and J. Dong, *J. Appl. Phys.*, 2010, **107**, 024306.
14 M. Blanchard, M. Lazzeri, F. Mauri and E. Balan, *Am. Mineral.*, 2008, **93**, 1019.
15 D. Karhánek, T. Bučko and J. Hafner, *J. Phys.: Condens. Matter*, 2010, **22**, 265006.
16 A. Davantès, D. Costa and G. Lefèvre, *J. Phys. Chem. C*, 2015, **119**, 12356–12364.
17 A. Davantès, D. Costa and G. Lefèvre, *J. Phys. Chem. C*, 2016, **120**, 11871–11881.
18 T. Würger, W. Heckel, K. Sellschopp, S. Müller, A. Stierle, Y. Wang, H. Noei and G. Feldbauer, *J. Phys. Chem. C*, 2018, **122**, 19481–19490.
19 B. Chiavarino, M. E. Crestoni, S. Fornarini, S. Taioli, I. Mancini and P. Tosi, *J. Chem. Phys.*, 2012, **137**, 024307.
20 A. E. J. Hoffman, L. Vanduyfhuys, I. Nevjestić, J. Wieme,

S. M. J. Rogge, H. Depauw, P. Van Der Voort, H. Vrielinck and V. Van Speybroeck, *J. Phys. Chem. C*, 2018, **122**, 2734–2746.
21 D. Fernández-Torre, R. Escribano, T. Archer, J. M. Pruneda and E. Artacho, *J. Phys. Chem. A*, 2004, **108**, 10535–10541.
22 B. Martín-Llorente, D. Fernández-Torre and R. Escribano, *ChemPhysChem*, 2009, **10**, 3229–3238.
23 Y. Kong, D. Hou, H.-D. Zhang, X. Zheng and R.-X. Xu, *J. Phys. Chem. C*, 2017, **121**, 18867–18875.
24 M. Katari, E. Nicol, V. Steinmetz, G. van der Rest, D. Carmichael and G. Frison, *Chem. Eur. J.*, 2017, **23**, 8414–8423.
25 M. Fanti, C.-A. Fustin, D. A. Leigh, A. Murphy, P. Rudolf, R. Caudano, R. Zamboni and F. Zerbetto, *J. Phys. Chem. A*, 1998, **102**, 5782.
26 G. Kresse and J. Furthmüller, *Phys. Rev. B*, 1996, **54**, 11169.
27 P. E. Blöchl, *Phys. Rev. B*, 1994, **50**, 17953.
28 G. Kresse and D. Joubert, *Phys. Rev. B*, 1999, **59**, 1758.
29 J. P. Perdew, K. Burke and M. Ernzerhof, *Phys. Rev. Lett.*, 1996, **77**, 3865.
30 S. Grimme, J. Antony, S. Ehrlich and H. Krieg, *J. Chem. Phys.*, 2010, **132**, 154104.
31 Crystallographic data available at: `https://dx.doi.org/10.5517/cc5d0k3`.
32 H. J. Monkhorst and J. D. Pack, *Phys. Rev. B*, 1976, **13**, 5188.
33 E. B. Wilson Jr., J. D. Decius and P. C. Cross, *Molecular Vibrations*, McGraw-Hill, 1955.
34 L. A. Woodward, *Introduction to the Theory of Molecular Vibrations and Vibrational Spectroscopy*, Oxford University Press, 1972.
35 D. Porezag and M. R. Pederson, *Phys. Rev. B*, 1996, **54**, 7830.
36 X. Gonze and C. Lee, *Phys. Rev. B*, 1997, **55**, 10355–10368.
37 S. Baroni, S. de Gironcoli, A. Dal Corso and P. Giannozzi, *Rev. Mod. Phys.*, 2001, **73**, 515–562.
38 M. Gajdoš, K. Hummer, G. Kresse, J. Furthmüller and F. Bechstedt, *Phys. Rev. B*, 2006, **73**, 045112.
39 N. B. Colthup, L. H. Daly and S. E. Wiberley, *Introduction to Infrared and Raman Spectroscopy*, Academic Press, 3rd edn, 1990.
40 T. Fornaro, M. Biczysko, S. Monti and V. Barone, *Phys. Chem. Chem. Phys.*, 2014, **16**, 10112–10128.
41 T. Fornaro, I. Carnimeo and M. Biczysko, *J. Phys. Chem. A*, 2015, **119**, 5313–5326.
42 T. Fornaro, D. Burini, M. Biczysko and V. Barone, *J. Phys. Chem. A*, 2015, **119**, 4224–4236.
43 J. B. O. Mitchell and S. L. Price, *Chem. Phys. Lett.*, 1991, **180**, 517–523.
44 D. A. Dixon, K. D. Dobbs and J. J. Valentini, *J. Phys. Chem.*, 1994, **98**, 13435–13439.
45 S. Scheiner, *Hydrogen Bonding: A Theoretical Perspective*, Oxford University Press, 1997.
46 J. R. Grover, E. A. Walters and E. T. Hui, *J. Phys. Chem.*, 1987, **91**, 3233–3237.
47 Y. C. Park and J. S. Lee, *J. Phys. Chem. A*, 2006, **110**, 5091–5095.
48 M. O. Sinnokrot and C. D. Sherrill, *J. Am. Chem. Soc.*, 2004, **126**, 7690–7697.
49 S. E. Wheeler and K. N. Houk, *J. Am. Chem. Soc.*, 2008, **130**, 10854–10855.
50 P. Larkin, *Infrared and Raman Spectroscopy*, Elsevier, 2011.
51 D. A. Leigh, K. Moody, J. P. Smart, K. J. Watson and A. M. Z. Slawin, *Angew. Chem. Int. Ed.*, 1996, **35**, 306.
52 C.-A. Fustin, D. A. Leigh, P. Rudolf, D. Timpel and F. Zerbetto, *ChemPhysChem*, 2000, **1**, 97.